ARID4B Promotes Lung Adenocarcinoma Malignancy by Activating *GPRC5C* transcription via Histone H1 Displacement

Guangnan Huang[1], Lei Gao[2,3], Shu Fang[3], Likun Xu[1], Xiaowei Zhao[4]

[1]Department of Respiratory and Critical Care Medicine, People's Hospital of Xinjiang Uygur Autonomous Region Bainiaohu Hospital (The Second Affiliated Hospital of Xi'an Jiaotong University Xinjiang Hospital), Urumqi, China

[2]Department of Endocrinology and Metabolic Diseases, The Second Affiliated Hospital of Xi'an Jiaotong University, Xi'an, China

[3]Department of General Medicine, People's Hospital of Xinjiang Uygur Autonomous Region Bainiaohu Hospital (The Second Affiliated Hospital of Xi'an Jiaotong University Xinjiang Hospital), Urumqi, China

[4]Hospital Office, People's Hospital of Xinjiang Uygur Autonomous Region Bainiaohu Hospital (The Second Affiliated Hospital of Xi'an Jiaotong University Xinjiang Hospital), Urumqi, China

Background: Epithelial–mesenchymal transition (EMT) and cancer cell stemness (CSC) are critical processes that driving the invasion and lethality of lung adenocarcinoma (LUAD). The chromatin remodeler *ARID4B* has been implicated in other cancers; however, its specific role and underlying mechanism in LUAD progression remain unclear.

Aims: This study aimed to elucidate the function of *ARID4B* in LUAD.

Study Design: This study integrated bioinformatics analysis, *in vitro* cellular functional assays, and *in vivo* orthotopic lung cancer models to investigate the oncogenic role of *ARID4B*.

Methods: *ARID4B* expression and its correlation with patient prognosis were analyzed using public databases. *ARID4B* was silenced using two independent short hairpin RNAs in A549 and H1650 LUAD cell lines, and subsequent changes in invasion, migration, and stemness markers were assessed. Tumor metastasis was evaluated using orthotopic and tail-vein injection mouse models. The regulatory mechanism by which *ARID4B* controls *GPRC5C* expression was investigated using dual-luciferase reporter and chromatin immunoprecipitation assays.

Results: *ARID4B* was significantly upregulated in LUAD and was associated with poor patient prognosis. Silencing *ARID4B* in LUAD cells significantly reduced their invasion and migration capabilities (adj. $p < 0.01$). Furthermore, *ARID4B* knockdown resulted in downregulation of SNAIL, upregulation of E-cadherin, and impairment of stem-like characteristics, as demonstrated by decreased CSC marker expression and reduced sphere-forming ability (adj. $p < 0.05$). In the orthotopic model, *ARID4B* deficiency markedly inhibited tumor metastasis (adj. $p < 0.001$). Mechanistically, *ARID4B* transcriptionally activated *GPRC5C* (adj. $p < 0.01$). Furthermore, *ARID4B* knockdown increased histone H1 occupancy at the *GPRC5C* promoter (adj. $p < 0.01$), indicating that *ARID4B* facilitates an open chromatin state. Rescue experiments further confirmed that *GPRC5C* is required for *ARID4B*-mediated maintenance of tumor invasiveness and cancer stemness.

Conclusion: *ARID4B* promotes LUAD malignancy by transcriptionally activating *GPRC5C*, thereby driving EMT and cancer stemness.

INTRODUCTION

Lung cancer remains the most prevalent and lethal malignancy worldwide, imposing a devastating global health burden, with non-small-cell lung cancer (NSCLC) accounting for 80–85% of all lung cancer cases.[1,2] Lung adenocarcinoma (LUAD) represents the most common histological subtype of NSCLC. Despite significant advancements in diagnostic techniques and therapeutic strategies in recent years, the prognosis of patients with LUAD remains dismal.[3] This highlights the urgent need to understand the molecular mechanisms driving LUAD progression, particularly those involved in metastasis. Epithelial–mesenchymal transition (EMT) and cancer stem cell (CSC) properties have emerged as key drivers of LUAD metastasis.[4,5] During EMT, cancer cells lose epithelial characteristics and acquire mesenchymal

Corresponding author: Lei Gao, Department of Endocrinology and Metabolic Diseases, The Second Affiliated Hospital of Xi'an Jiaotong University, Xi'an, China; Department of General Medicine, People's Hospital of Xinjiang Uygur Autonomous Region Bainiaohu Hospital (The Second Affiliated Hospital of Xi'an Jiaotong University Xinjiang Hospital), Urumqi, China

e-mail: 012160_gao@163.com

Received: November 20, 2025 **Accepted:** January 15, 2026 **Available Online Date:** • **DOI:** 10.4274/balkanmedj.galenos.2026.2025-10-260

Available at www.balkanmedicaljournal.org

ORCID iDs of the authors: G.H. 0000-0002-5088-8170; S.F. 0009-0004-4462-1447; L.X. 0009-0007-2630-655X; X.Z. 0009-0006-1101-1786; L.G. 0009-0000-5277-7178.

Cite this article as: Huang G, Fang S, Xu L, Zhao X, Gao L. *ARID4B* Promotes Lung Adenocarcinoma Malignancy by Activating *GPRC5C* transcription via Histone H1 Displacement. Balkan Med J.; 2026; 43(3):

traits, thereby significantly enhancing their invasive and migratory capacities.[5] CSCs, a small subpopulation of tumor cells with stem-like features, are closely associated with EMT; EMT can enrich CSC-like cells, which subsequently contribute to tumor initiation, metastasis, and resistance to therapy.[6,7] Notably, the simultaneous inhibition of EMT and CSC properties has been shown to attenuate LUAD progression in preclinical models,[8] highlighting these processes as promising therapeutic targets.

Chromatin remodeling proteins dynamically regulate gene expression by altering DNA–histone packaging without changing the underlying DNA sequence and are increasingly implicated in tumorigenesis.[9,10] *ARID4B* (AT-Rich Interaction Domain 4B), a member of the ARID family of chromatin remodeling proteins, plays oncogenic roles in multiple solid tumors and is aberrantly expressed in cancers such as breast, colorectal, and prostate cancer.[11,12] *ARID4B* can activate transcription by displacing the repressive linker histone H1, a protein that stabilizes condensed chromatin and represses gene expression, from target gene promoters. This results in a more open chromatin structure and promotes mammary tumor growth and metastasis in mice, while also sustaining proliferation in PTEN-deficient prostate cancer.[13,14] Bioinformatic analyses have suggested that *ARID4B* is upregulated in LUAD tissues. However, although these mechanisms have been characterized in other malignancies, the functional relevance of *ARID4B* and its specific molecular partners in the context of LUAD remain to be established.

Intriguingly, prior chromatin immunoprecipitation (ChIP)-seq studies in prostate cancer identified *GPRC5C* (G Protein-Coupled Receptor Class C Group 5 Member C) as a potential downstream target of *ARID4B*, with *ARID4B* binding to the *GPRC5C* promoter.[13] *GPRC5C,* a member of the G protein-coupled receptor family, exhibits broad pro-tumorigenic effects in other malignancies, for instance, by enhancing the survival of leukemia stem cells and promoting pancreatic cancer cell invasion.[15,16] Similar to *ARID4B, GPRC5C* is upregulated in LUAD tissues; however, its role in LUAD progression has not yet been investigated. Based on these observations, we hypothesized that *ARID4B* may, at least in part, contribute to the malignant development of LUAD by transcriptionally regulating the expression of *GPRC5C*.

This study aims to address this significant knowledge gap. We will systematically investigate the role of *ARID4B* in regulating LUAD cell stemness and EMT. Furthermore, we will delineate the mechanistic relationship between *ARID4B* and *GPRC5C*.

MATERIALS AND METHODS

Workflow description: This study was designed to investigate the oncogenic role of *ARID4B* in LUAD through an integrated workflow combining bioinformatics analysis, *in vitro* functional assays, and *in vivo* mouse models, followed by mechanistic exploration using luciferase reporter and ChIP assays to examine *ARID4B*-mediated transcriptional regulation of *GPRC5C*, with rescue experiments ultimately validating *GPRC5C* as a critical downstream effector of *ARID4B*-driven malignancy.

Data acquisition

The mRNA expression profile of *ARID4B* in LUAD (n = 515 tumor vs. 59 normal samples) was obtained from the UALCAN database (https://ualcan.path.uab.edu/analysis.html). Data on ARID4B protein expression in LUAD (n = 111 tumor samples vs. 102 normal samples) were obtained from the cProSite database (https://cprosite.ccr.cancer.gov/). Differences in mRNA and protein-levels were evaluated using Student's t-test. Expression data for *ARID4B* in clinical LUAD tissues were also downloaded from the THPA database (https://www.proteinatlas.org/). The correlation between *ARID4B* mRNA expression and patient overall survival (OS) was analyzed by pooling data from five independent GEO datasets: GSE31210 (n = 226), GSE10425 (n = 40), GSE14814 (n = 71), GSE26939 (n = 115) and GSE13213 (n = 117). A fixed-effects meta-analysis was performed using the LOGpc online tool (https://bioinfo.henu.edu.cn/DatabaseList.jsp), employing a Kaplan–Meier estimator with a log-rank test. The cut-off value for defining high- and low- expression groups was set at the median *ARID4B* expression level. Hazard ratios and 95% confidence intervals were calculated using the Cox proportional hazards model.

Cell culture

The lung cancer cell line A549 was cultured in F-12K medium (Servicebio, Wuhan, China) supplemented with 10% fetal bovine serum (FBS) (Tianhang Biotechnology, Huzhou, China). The H1650 cell line was cultured in RPMI-1640 medium (Solarbio, Beijing, China) supplemented with 10% FBS. Both cell lines were obtained from iCell Bioscience Inc (Shanghai, China) and maintained at 37 °C in a humidified incubator with 5% CO_2.

Cells were seeded and cultured according to designated grouping until adherence. The cells were cultured in medium containing the virus and virus dosage were optimized for preliminary experiments to determine multiplicities of infection values. After culturing the infected cells for 48 hours, puromycin (2 μg/mL) was added for selection. The culture medium was replaced every other day until all cells in the uninfected control group had died. Subsequently, puromycin was removed, and the infected cells were continuously expanded through routine medium replacement.

Lentiviral construction and cell infection

The lentiviral vectors expressing short hairpin RNAs targeting *ARID4B* were constructed by inserting oligonucleotides targeting the human *ARID4B* sequence (NM_016374) into the pLVX-shRNA1 vector (Fenghui Biotechnology, China) at the BamHI and EcoRI restriction sites. The targeting sequences were 5'-CCTATTAACAAACGACCTGTA-3' (shARID4B-1) and 5'-GCAATACAGAAGAGTGTCTAA-3' (shARID4B-2). For virus production, HEK293T cells were cultured in DMEM (Biosharp, China) supplemented with 10% FBS and co-transfected at 60% confluence in 10 cm dishes with 14 μg of the shRNA-expressing lentiviral plasmid, 10.5 μg of the packaging plasmid psPAX2 (Fenghui, China), and 3.5 μg of the envelope plasmid pMD2.G (Fenghui, China) using Lipofectamine 3000 (Invitrogen, USA). The culture supernatants were harvested 48 h post-transfection, filtered through 0.45 μm filters, and concentrated by ultracentrifugation at

72,000 × g for 120 min. The viral pellets were resuspended, and titers were determined as follows: Lv-shNC, 3.1×10^8 TU/mL, Lv-shARID4B-1, 2.5×10^8 TU/mL, Lv-shARID4B-2, 2.8×10^8 TU/mL. A549 and H1650 cells were then transduced with these lentiviruses and selected with 2 μg/mL puromycin to establish stable *ARID4B*-knockdown cell lines.

Real-time polymerase chain reaction

Total RNA was isolated using TRIpure reagent (BioTeke, Beijing, China) from three independently cultured and transfected cell samples (biological replicates, n = 3), and RNA concentration was measured using a Nano2000 spectrophotometer. cDNA was synthesized with the All-in-One First-Strand cDNA Synthesis SuperMix (Magen, Guangzhou, China). Quantitative polymerase chain reaction (PCR) was measured in quadruplicate (technical replicates) on the Pangaea 3 instrument (Aperbio, Suzhou, China) using the following reaction mixture: 1 μL cDNA, 0.5 μL each of forward and reverse primers (10 μM), 10 μL of 2 × Taq PCR MasterMix, 0.3 μL SYBR Green, and nuclease-free water to a final volume of 20 μL. The thermal cycling conditions were as follows: initial denaturation at 95 °C for 5 min, followed by 40 cycles of 95 °C for 10 s and 60 °C for 10 s. Relative gene expression levels were calculated using the $2^{-\Delta\Delta Ct}$ method. The primer sequences used in this study were as follows: *ARID4B* forward, 5'-CCCCTCCTACTACACCT-3', reverse, 5'-CAACACTATCCACCTCAA-3'. GPRC5C forward, 5'-CTGCTGGGTGCCTTCCT-3', reverse, 5'-TGTTGTGCTGCTTGTTGC-3'.

Western blot

Total protein was extracted using ice-cold lysis buffer (Proteintech, Wuhan, China) containing 1 mM phenylmethylsulfonyl fluoride (PMSF), followed by centrifugation at 10,000 × g for 5 min. Protein concentration was measured using a BCA assay with BSA as the standard. Equal amounts of protein were separated by SDS-PAGE (Proteintech) and transferred onto PVDF membranes (Thermo Fisher Scientific, USA). After blocking for 1 h at room temperature, membranes were incubated overnight at 4 °C with the following primary antibodies: anti-*ARID4B* (1:1000, Proteintech), anti-*CD133* (1:500, Zenbio, Chengdu, China), anti-*OCT4* (1:500, Zenbio), anti-*SOX2* (1:500, Zenbio), anti-GPRC5C (1:500, Abcept, Suzhou, China), anti-SNAIL (1:500, Zenbio), and anti-E-cadherin (1:500, Zenbio). After washing, membranes were incubated with HRP-conjugated secondary antibodies (diluted 1:10,000) for 40 min at 37 °C. Protein bands were detected using an ECL detection system and imaged. Band densities were analyzed using Gel-Pro-Analyzer software.

Sphere formation assay

Cells were seeded into a 48-well plate (Labselect, Beijing, China) and cultured in medium containing 0.5% methylcellulose (Macklin, Shanghai, China), N2 supplement (Biosharp, Hefei, China), 20 ng/mL EGF (MCE, USA), and 20 ng/mL bFHF (MCE, USA). After 14 days of culture, sphere formation was examined under a microscope (Olympus, Tokyo, Japan). Spheres with diameters greater than 75 μm were counted and imaged. Assays were performed using cells from three independent cultures (biological replicates, n = 3), and the average value of each biological replicate was used for statistical analysis.

Wound-healing assay

After 48 h of culture, A549 and H1650 cells with stable *ARID4B* knockdown were pre-treated with (MCE, USA) in serum-free medium for 1 h. A linear wound was then created in each well using a sterile pipette tip, and the initial wound area was imaged under a microscope. Following incubation in serum-free medium for 24 h, cells were photographed again to assess migratory ability. Assays were performed using cells from three independent cultures (biological replicates, n = 3), and the average value per biological replicate was used for statistical analysis.

Transwell assay

Transwell chambers precoated with Matrigel (Corning, Corning, NY, USA) were placed in 24-well plates. The lower chambers were filled with 800 μL medium containing 10% FBS, while 200 μL cell suspension was added to the upper chambers. After 24 h of incubation, the chambers were washed with phosphate buffered saline (PBS). Cells were then fixed with 4% paraformaldehyde (Aladdin, Shanghai, China) for 20 min and stained with crystal violet (Macklin, Shanghai, China) for 2 min. Invasive cells on the lower surface of the membrane were observed, imaged, and counted using a microscope. Assays were performed using cells from three independent cultures (biological replicates, n = 3), and the average value per biological replicate was used for statistical analysis.

Immunofluorescence assay

Cells grown on slides were fixed with 4% paraformaldehyde for 15 min, permeabilized with 0.1% Triton X100 (Beyotime, Shanghai, China) for 30 min, and blocked with 1% BSA (Sangon Biotech, Shanghai, China) for 15 min. Slides were then incubated overnight at 4 °C with primary antibodies against E-cadherin (340341, Zenbio) and SNAIL (340942, Zenbio) at a dilution of 1:100. After washing, slides were incubated with Cy3conjugated goat antirabbit immunoglobulin G (IgG) (SA00009-2, Proteintech) diluted 1:200 for 60 min in the dark. Nuclei were counterstained with DAPI (Aladdin), and slides were mounted with antifading medium (Solarbio) before observation and imaging under a microscope.

Tumor xenograft transplantation

Model 1: Seven-week-old BALB/c nude mice were randomly divided into two groups (shNC and shARID4B, biological replicates, n = 6). After one week of acclimation, 1×10^6 H1640 cells were orthotopically injected into the left lung of each mouse. The injection site was located 1.5 cm above the lower rib line, directly below the inferior margin of the scapula along the axilla–back line. A needle was rapidly inserted 5–7 mm into the thoracic cavity, and the cell suspension was delivered. Following injection, mice were placed in the left lateral position and continuously monitored for 45–60 min until full recovery. Four weeks after injection, both left and right lungs were imaged and quantitatively analyzed using a small–animal bioluminescence imaging system.

Model 2: In a separate experimental model, seven-week-old BALB/c nude mice were randomly allocated to two groups (shNC and shARID4B, biological replicates, n = 6). A total of 5×10^6

cells were resuspended in 300 µL serum-free RPMI medium and administered via tail-vein injection. Bioluminescence imaging and quantitative analysis were performed five weeks post-injection. After acclimatization, each mouse was assigned a unique identification number and randomly allocated to experimental groups using a random number sequence by a researcher who was not involved in subsequent injections or data analysis. To minimize observer bias, investigators responsible for *in vivo* bioluminescence imaging, image quantification, and histological assessment were blinded to group allocation throughout the study. During imaging and tissue processing, mice were identified solely by their unique ID numbers. No animals were excluded after randomization, and all mice subjected to orthotopic or tail-vein injection survived until the predetermined experimental endpoint and were included in the final analysis. This study was approved by the Clinical Research Ethics Committee of the People's Hospital of Xinjiang Uygur Autonomous Region (approval number: KY2024052105; date: 21.05.2024).

Hematoxylin-eosin staining

Tissue sections were deparaffinized and rehydrated, followed by staining with hematoxylin (Solarbio) for 5 min. Sections were differentiated using acid alcohol and rinsed thoroughly with tap water for 20 min. Cytoplasmic staining was performed with eosin Y solution (Sangon Biotech) for an additional 5 min. After dehydration and clearing in xylene, sections were mounted with neutral resin and coverslipped. Finally, stained sections were examined and imaged using a light microscope.

Luciferase reporter assay

HEK293T cells were cultured in DMEM (Servicebio) supplemented with 10% FBS at 37 °C in a 5% CO_2 incubator. For transfection, cells were seeded into 12-well plates and transfected using Lipofectamine 3000 (Invitrogen, CA, USA) with a combination of pGL3basic or pGL3-GPRC5C promoter vectors and either siNC or siARID4B constructs. After 48 h, relative luciferase activity was measured using a multimode microplate reader. Luciferase activity was calculated by normalizing firefly luciferase luminescence to Renilla luciferase signal for each well (Firefly/Renilla ratio) to control for transfection efficiency. The normalized luciferase activity for each experimental group was expressed as fold change relative to the mean value of the control group (siNC + pGL3-GPRC5C promoter), which was defined as 1.0. Data are presented as the mean ± standard deviation (SD) from three independent transfection experiments (biological replicates).

Chromatin immunoprecipitation-polymerase chain reaction

Cells were crosslinked with 1% formaldehyde for 10 min at 37 °C, and the reaction was quenched by the addition of glycine. Cells were then washed with ice-cold PBS containing PMSF, lysed in SDS lysis buffer, and chromatin was sheared by sonication. Immunoprecipitation was performed overnight at 4 °C using specific antibodies or control IgG. Immune complexes were captured with Protein A/G Agarose, followed by sequential washing and elution with elution buffer. Cross-links were reversed by incubation with NaCl at 65 °C, samples were subsequently digested with proteinase K. DNA was purified by phenol-chloroform extraction and ethanol precipitation, then resuspended in TE buffer. PCR amplification was performed using gene-specific primers. Data were presented as fold enrichment relative to IgG control (mean ± SD) from three independent chromatin preparations (biological replicates). The primer sequences used were as follows: *GPRC5C* forward: 5'GGACCGTGCGTGCAAAAG3', GPRC5C reverse: 5'GGCACAGTTCGCTGGGAG3'.

Statistical analysis

Statistical analyses were conducted using GraphPad Prism 9.0. Data are expressed as the mean ± SD. Sample sizes for *in vivo* experiments (n = 6 per group) and *in vitro* experiments (n = 3 biological replicates) were determined based on feasibility and commonly accepted practices in the field. For *in vitro* experiments, assays were performed using cells from three independent cultures (biological replicates, n = 3), and the average value per biological replicate was used for statistical analysis. No formal a priori power analysis was conducted, and this limitation should be considered when interpreting the statistical results, particularly for outcomes with modest effect sizes. Differences between two groups were assessed using an unpaired Student's t-test. Comparisons involving more than two groups were analyzed using one-way analysis of variance, followed by Tukey's post-hoc test for multiple comparisons. For experiments involving multiple comparisons, p values were adjusted using the Bonferroni correction. An adjusted p value of 0.05 was considered statistically significant.

RESULTS

ARID4B is highly expressed in lung adenocarcinoma and predicts a poor prognosis

Bioinformatic analysis revealed that *ARID4B* is significantly upregulated in LUAD. Specifically, analysis of the UALCAN database indicated elevated *ARID4B* mRNA expression in LUAD tissues compared with normal lung tissues ($p < 0.0001$, Figure 1a). Consistently, proteomic data obtained from the cProSite database demonstrated significantly higher *ARID4B* protein levels in LUAD samples ($p < 0.0001$, Figure 1b). In addition, immunohistochemical images from the THPA database further confirmed increased *ARID4B* expression in clinical LUAD specimens (Figure 1c). Subsequent survival analysis using the LOGpc database revealed a significant association between high *ARID4B* expression and reduced OS in patients with LUAD ($p = 5e{-}04$, GSE31210; $p = 0.0124$, GSE26939; $p = 0.0283$, GSE14814; $p = 0.0023$, GSE13213; $p = 0.0138$, GSE10245; Figure 1d). Collectively, these results indicate that *ARID4B* is overexpressed in LUAD and is closely associated with poor prognosis in LUAD.

Knockdown of ARID4B inhibits the stemness of LUAD cells

In A549 and H1650 cells, stable transduction with shARID4B-1 or shARID4B-2 significantly reduced *ARID4B* mRNA and protein expression levels (Figures 2a and b). In A549 cells, *ARID4B* expression was decreased by approximately 4.6-fold and 3.3-fold (adj. $p < 0.001$). In H1650 cells, *ARID4B* expression was decreased by approximately 4.7-fold and 3.2-fold (adj. $p < 0.001$), respectively. As shown in

Figure 2c, *ARID4B* depletion resulted in marked downregulation of the stem cell-associated surface markers *CD133*, as well as the stem cell-related transcription factors *SOX2* and *OCT4*, indicating suppression of CSC characteristics. Furthermore, knockdown of *ARID4B* significantly impaired the sphere-forming capacity of LUAD cells (Figure 2d). In A549 cells, the average number of tumor spheres reduced from 102.0 ± 13.5 in the shNC group to 44.0 ± 9.2 in the shARID4B-1 group (−56.9%, adj. p = 0.0025) and to 47.7 ± 9.8 in the shARID4B-2 group (−53.2%, adj. p = 0.0038). Similarly, in H1650 cells, sphere formation was decreased from 107.0 ± 17.1 (shNC) to 46.7 ± 12.5 (shARID4B-1; −56.4%, adj. p = 0.0221) and to 48.3 ± 12.5 (shARID4B-2; −54.9%, adj. p = 0.0255). These results indicate that *ARID4B* is essential for maintaining the clonogenic capacity and stem-like growth properties of LUAD cells.

Knockdown of ARID4B inhibits invasion and epithelial–mesenchymal transition in LUAD cells

As shown in Figure 3a, knockdown of *ARID4B* significantly suppressed the migratory capacity of LUAD cells. In A549 cells, the wound closure rate reduced from an average of 51.69% ± 5.06% in the shNC group to 23.76% ± 3.27% in the shARID4B-1 group (−54.0%, adj. p = *0.0008*) and to 25.89% ± 3.40% in the shARID4B-2 group (−49.9%, adj. p = 0.0014). A comparable inhibitory effect was observed in H1650 cells, in which the migration rate was decreased from 48.75% ± 5.46% (shNC) to 28.25% ± 3.17% (shARID4B-1; −42.1%, adj. p = 0.0017) and to 29.32% ± 3.50% (shARID4B-2; −39.9%, adj. p = 0.0024). Consistent with these findings, *ARID4B* silencing markedly impaired the invasive potential of LUAD cells (Figure 3b). In A549 cells, the number of invading cells was decreased from 109.53 ± 13.49 (shNC) to 53.20 ± 1.50 (shARID4B-1; −51.4%, adj. p = 0.0002) and to 53.93 ± 3.10 (shARID4B-2; −50.8%, adj. p = 0.0003). Likewise, invasion of H1650 cells reduced from 70.73 ± 3.72 (shNC) to 29.80 ± 3.44 (shARID4B-1; −57.9%, adj. p < 0.0001) and to 27.33 ± 5.41 (shARID4B-2; −61.4%, adj. p < 0.0001). Furthermore, immunofluorescence staining indicated that depletion of *ARID4B* resulted in increased expression of E-cadherin and decreased expression of SNAIL in both lung cancer cells (Figures 4a and b). Overall, these results demonstrate that *ARID4B* induces LUAD cell migration, invasion, and EMT.

Knockdown of ARID4B inhibits the invasion of LUAD cells in vivo

To investigate the role of *ARID4B* in intrapulmonary metastasis, H1650 cells were injected into the left lung of nude mice. A

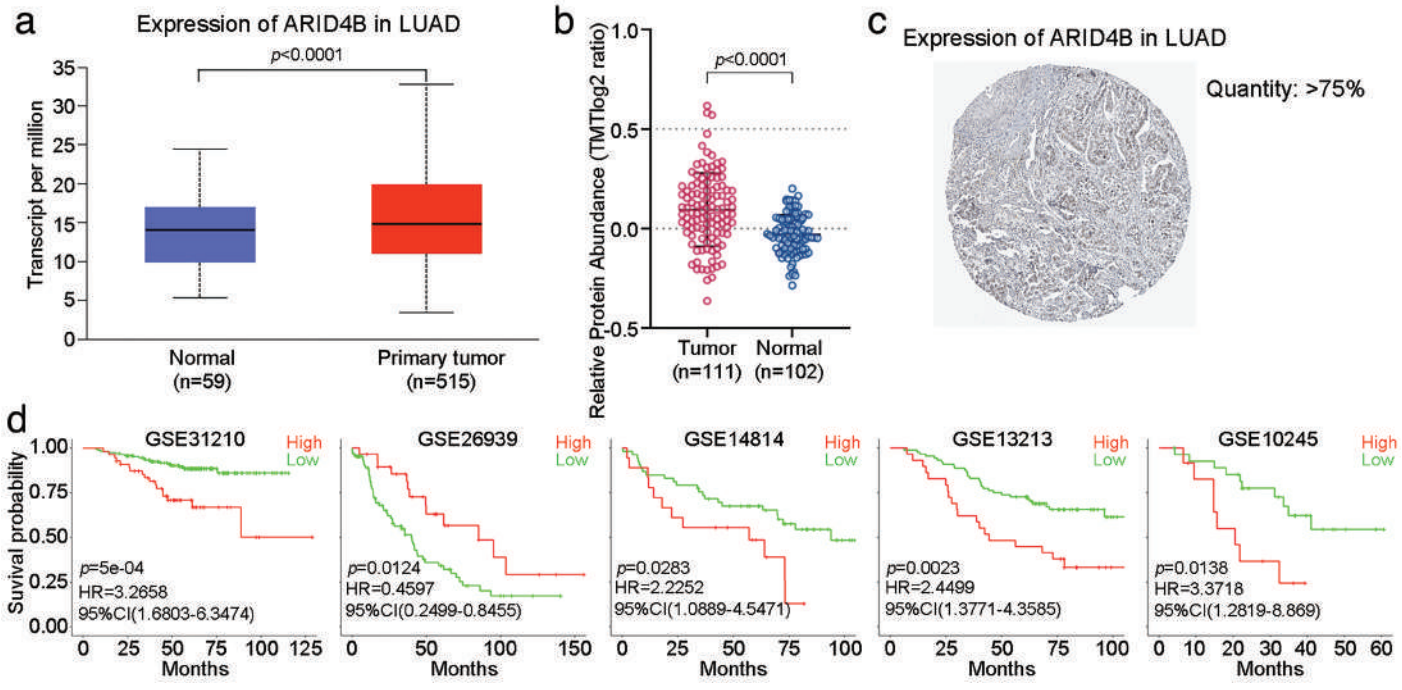

FIG.1. *ARID4B* is highly expressed in lung adenocarcinoma (LUAD) and predicts a poor prognosis. (a) The mRNA expression profile of *ARID4B* in LUAD (n = 515 tumor vs. 59 normal samples) was presented by the UALCAN data analysis. (b) The data of *ARID4B* protein expression in LUAD (n = 111 tumor vs. 102 normal samples) was obtained from the cProSite. (c) The expression of *ARID4B* in clinical LUAD tissues were downloaded from THPA database. (d) The correlation between *ARID4B* mRNA expression and patient overall survival was analyzed by pooling data from five independent gene expression omnibus datasets: GSE31210 (n = 226), GSE10425 (n = 40), GSE14814 (n = 71), GSE26939 (n = 115), and GSE13213 (n = 117). A fixed-effects meta-analysis was p erformed using the LOGpc online tool. The hazard ratio (HR) and 95% confidence interval for each dataset were calculated using a univariate Cox proportional hazards model, with patients dichotomized into high- and low-expression groups based on the median *ARID4B* expression level within each cohort. The pooled HR and its significance were then derived, and the overall survival difference was assessed using the log-rank test.

CI, confidence interval.

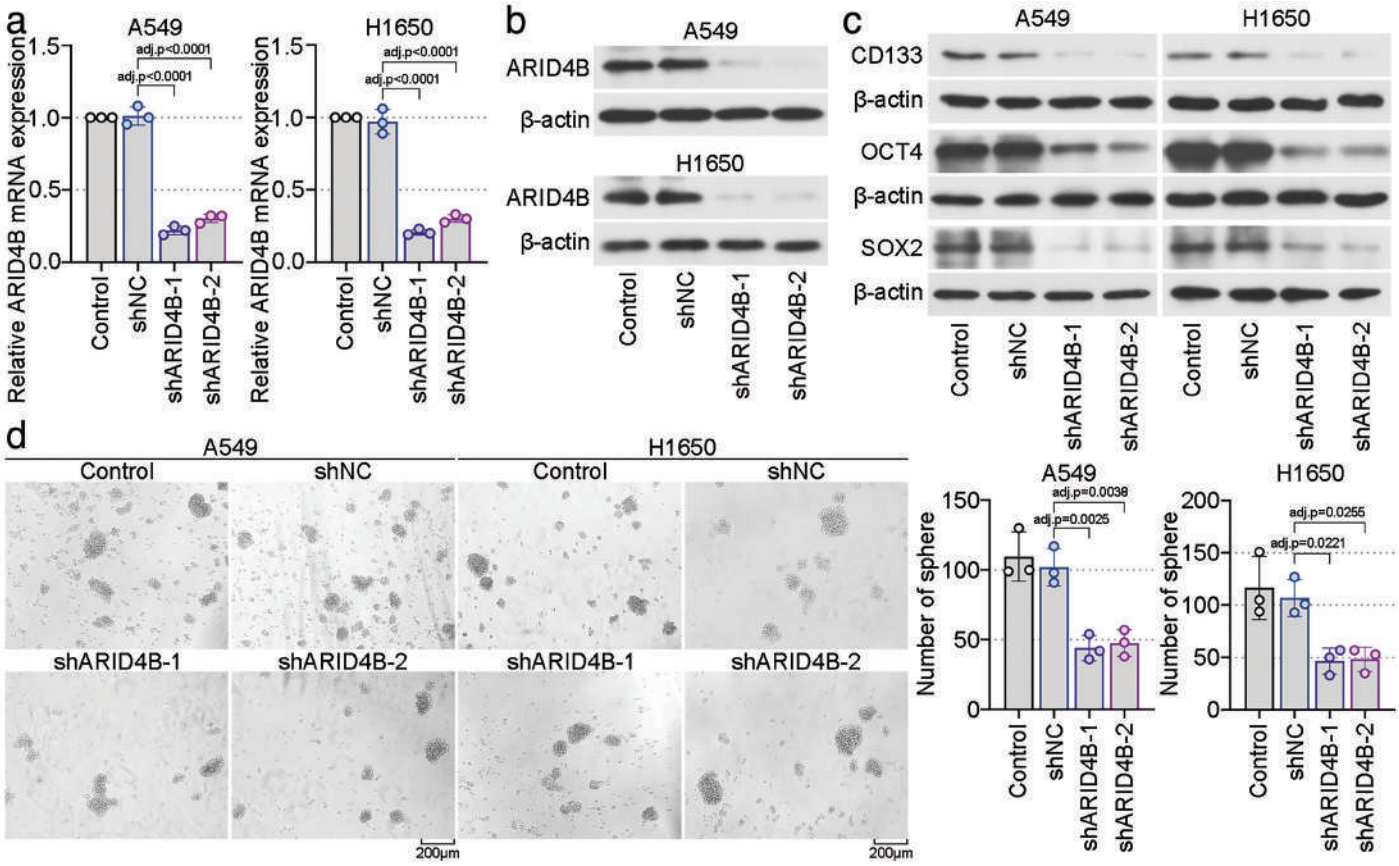

FIG. 2. Knockdown of *ARID4B* inhibits the stemness of lung adenocarcinoma cells. (a, b) The lentivirus-based systems were applied to knockdown *ARID4B* in A549 and H1650 cells, respectively, and screened for stably transfected cell lines. Real-time PCR and Western blot analysis of *ARID4B* expression in tumor cells. (c) Western blot analysis of *CD133*, *OCT4* and *SOX2* expression in tumor cells. (d) Images and the statistical results showed the effect of *ARID4B* knockdown on the spheres formation abilities of cancer cell stemness by sphere-forming assay. Scale bar indicates 200 μm. Data are expressed as mean ± standard deviation (n = 3, biological replicates). Comparisons among multiple groups were performed by one-way ANOVA followed by Tukey's post-hoc test; the *p* values shown in the figure are adjusted *p* values (adj. *p*) after Bonferroni correction.

schematic diagram of primary tumor formation in the left lung and local metastasis to the right lung is shown in Figure 5a. As shown in Figure 5b, knockdown of *ARID4B* significantly inhibited primary tumor growth. Specifically, the bioluminescence signal intensity in the left lung was reduced from 1.63 ± 0.41 (× 10^7 p/s/cm²/sr) in the shNC group to 0.74 ± 0.12 in the shARID4B group (−54.7%, adj. $p = 0.0002$). Concurrently, spontaneous local metastases to the right lung was markedly attenuated, with bioluminescence signal intensity decreasing from 1.22 ± 0.15 to 0.43 ± 0.11 (−64.9%, adj. $p = 0.0002$). Consistent with these findings, *ARID4B* silencing also potently suppressed distant metastases in a tail-vein injection model (Figure 5c). The total metastatic burden was reduced from 5.33 ± 1.52 (× 10^6 p/s/cm²/sr) in the shNC group to 1.28 ± 0.32 in the shARID4B group, corresponding to a 76.0% inhibition (adj. $p < 0.0001$). In addition, hematoxylin and eosin staining of lung sections revealed that shARID4B markedly reduced the number and size of metastatic tumor foci compared with the shNC group (Figure 5d). These findings collectively demonstrated that *ARID4B* silencing effectively suppresses LUAD tumor growth and metastatic potential.

ARID4B promotes the transcriptional activation of GPRC5C

To elucidate the mechanistic relationship between *ARID4B* and its putative downstream target *GPRC5C*, we first examined whether *ARID4B* knockdown significantly reduced both the mRNA and protein expression levels of *GPRC5C* (Figure 6a and b). In A549 cells, shARID4B-1 and shARID4B-2 reduced *GPRC5C* mRNA expression to approximately 21.0% (adj. $p < 0.0001$) and 26.1% (adj. $p < 0.0001$) of the shNC control, respectively. Similar effects were observed in H1650 cells, in which *GPRC5C* expression was reduced to 20.6% (shARID4B-1, adj. $p < 0.0001$) and 25.3% (shARID4B-2, adj. $p < 0.0001$) of control levels. We next performed dual-luciferase reporter assay to assess whether *ARID4B* regulates *GPRC5C* at the transcriptional level. Compared with the activity of the *GPRC5C* promoter construct in siNC-transfected cells, co-transfection with *ARID4B*-targeting siRNAs significantly reduced promoter activity to 50.7% (siRNA1, adj. $p = 0.0006$) and 56.1% (siRNA2, adj. $p = 0.0014$) (Figure 6c). These results indicate that *ARID4B* is required for efficient transcriptional activation of the *GPRC5C* promoter. To further validate the direct interaction between *ARID4B* and the

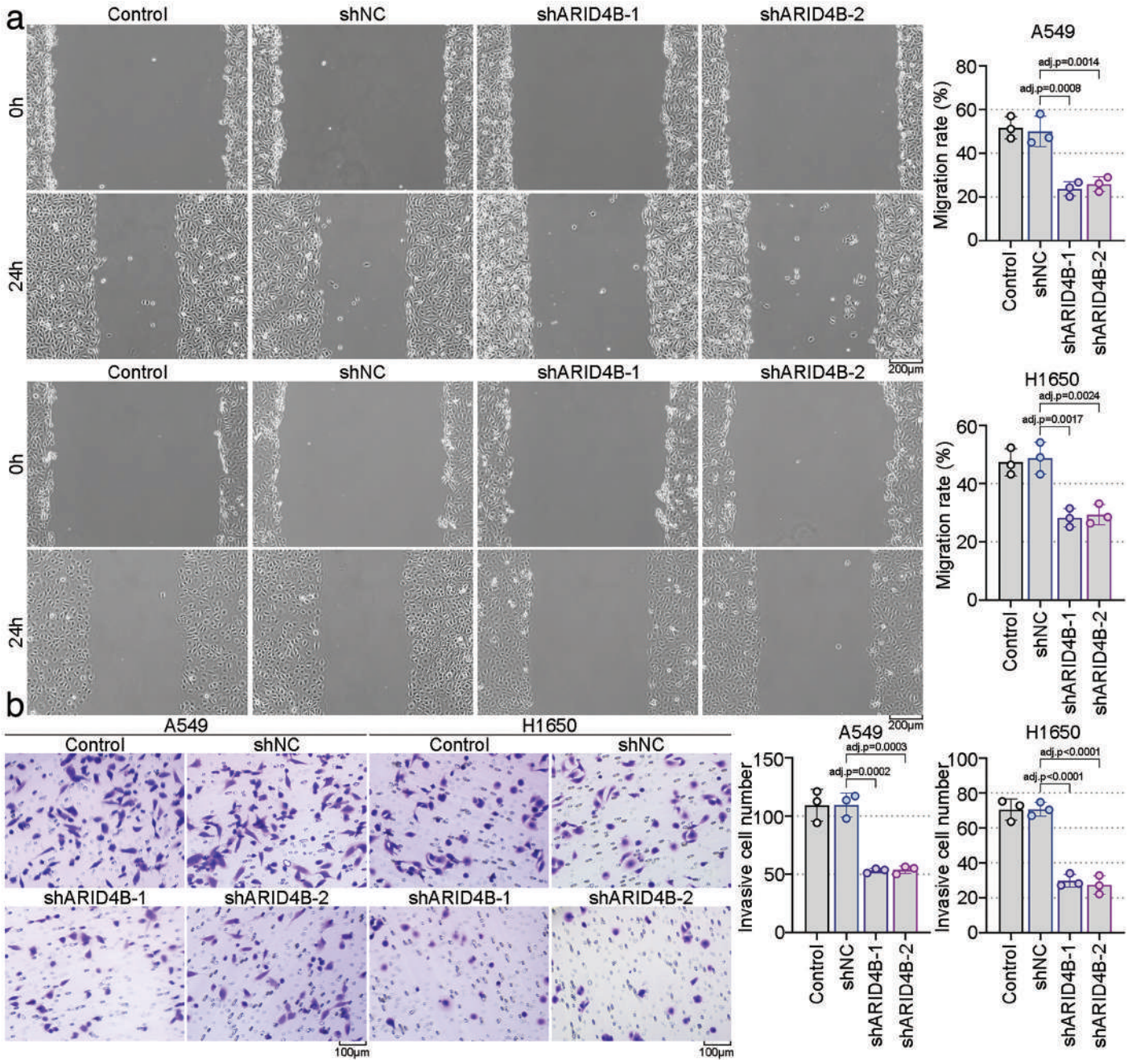

FIG. 3. Knockdown of *ARID4B* inhibits the invasion and epithelial-mesenchymal transition of lung adenocarcinoma (LUAD) cells. (a) The effect of *ARID4B* on the migration of LUAD cells by wound-healing assay. Photographs showed cell migration before and after injury under the microscope at 100 × magnification field. Quantification of cell migration by measuring wound closure areas before and after injury. (b) The effect of *ARID4B* on the invasion of LUAD cells by transwell assay (crystal violet staining × 200). Data are expressed as mean ± standard deviation (n = 3, biological replicates). Comparisons among multiple groups were performed by one-way ANOVA followed by Tukey's post-hoc test; the *p* values shown in the figure are adjusted *p* values (adj. *p*) after Bonferroni correction.

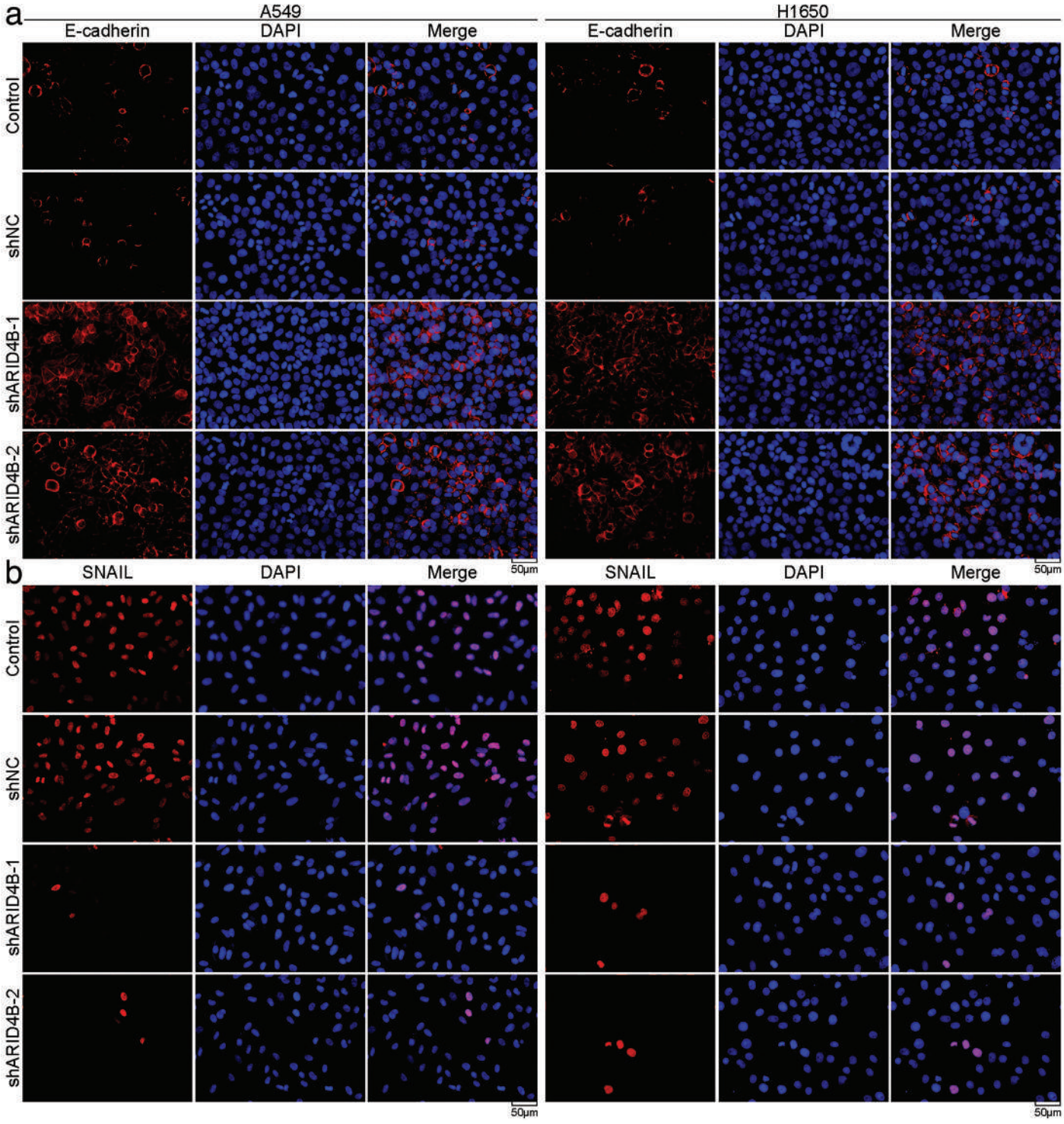

FIG. 4. Knockdown of *ARID4B* down-regulates the expression of markers for epithelial-mesenchymal transition. (a, b) Representative immunofluorescence images of E-cadherin and SNAIL expression (red) in tumor cells. Cell nuclei were stained by DAPI (blue). Scale bar indicates 50 μm.

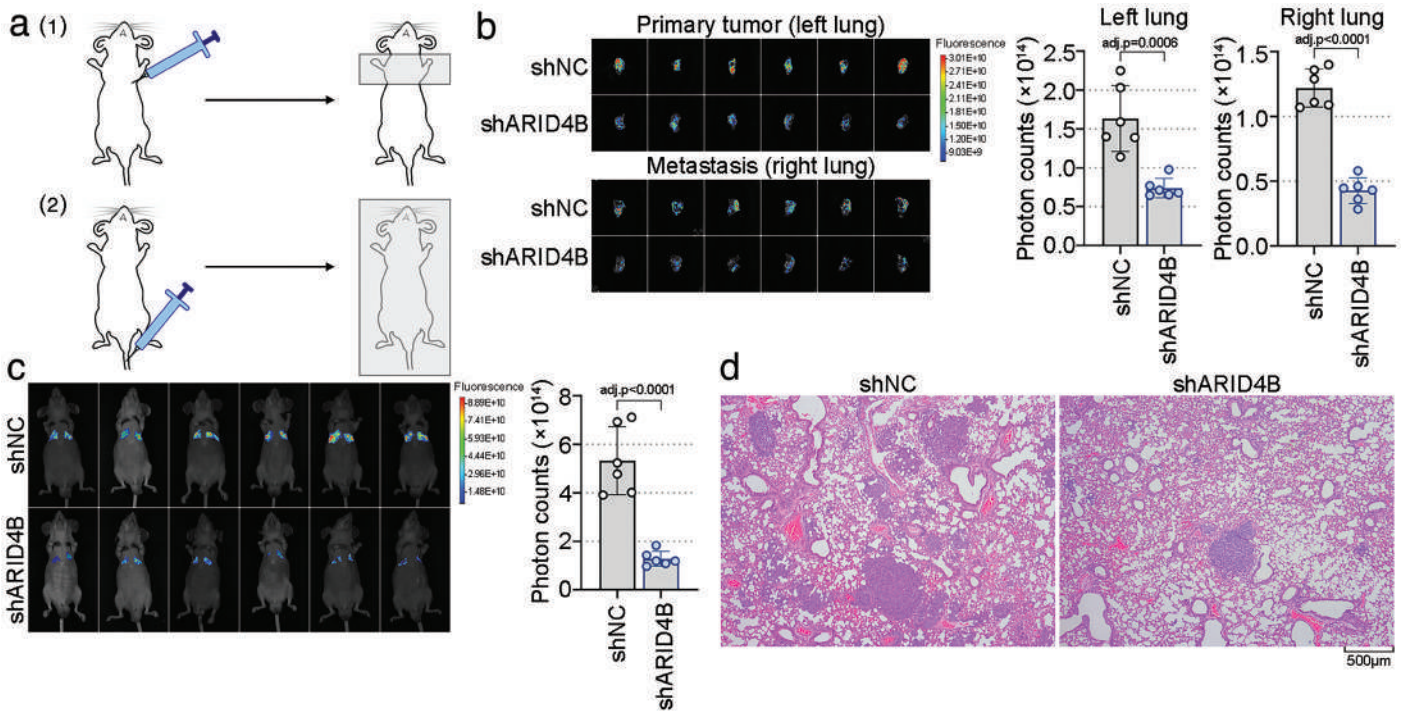

FIG. 5. Knockdown of *ARID4B* inhibits the invasion of lung adenocarcinoma cells *in vivo*. (a) Experimental schematic diagram of lung metastasis and xenograft colonization in mice. (b) Bioluminescence images of BALB/c nude mice after orthotopic injection of H1650 cells with *ARID4B* knockdown and quantitation of imaging data. (c) Bioluminescence images of xenograft mice and quantitation of imaging data. (d) The metastasis of lung tissue was detected by hematoxylin and eosin staining. Scale bar indicates 500 μm. Data are expressed as mean ± standard deviation (n = 6, biological replicates). Differences between two groups were assessed using an unpaired Student's t-test; the *p* values shown in the figure are adjusted *p* values (adj. *p*) after Bonferroni correction.

GPRC5C promoter, ChIP assays were performed. As shown in Figure 6d, the target promoter region exhibited specific enrichment in anti-*ARID4B* immunoprecipitates compared with the IgG control (Figure 6d). Notably, knockdown of *ARID4B* significantly increased histone H1 binding to the *GPRC5C* promoter. In A549 cells, histone H1 enrichment elevated by approximately 2.0-fold in the Lv-shARID4B-1 group and 1.5-fold in the Lv-shARID4B-2 group relative to the Lv-shNC control (both adj. $p < 0.0001$) (Figure 6e). A similar trend was observed in H1650 cells. These findings suggest that *ARID4B* promotes *GPRC5C* transcription by reducing histone H1 binding at the promoter, thereby facilitating a more open chromatin configuration. A schematic model summarizing the proposed mechanism is shown in Figure 6f.

ARID4B regulates GPRC5C expression to influence the malignant phenotype of LUAD cells

To determine whether *GPRC5C* functions as a downstream effector of *ARID4B*, rescue experiments were performed in H1650 cells with stable *ARID4B* knockdown. Overexpression of *GPRC5C* effectively restored its protein expression in *ARID4B* deficient cells (Figure 7a). Notably, the downregulation of stemness-associated markers induced by *ARID4B* knockdown was significantly reversed following *GPRC5C* overexpression (Figure 7b). Functionally, restoration of *GPRC5C* largely rescued the impaired migratory capacity caused by *ARID4B* deficiency. In woundhealing assay, the migration rate reduced from 48.45% ± 6.02% in the LvshNC + Vector group to 28.67% ± 3.57% in the LvshARID4B + Vector group (−40.8%, adj. $p = 0.0073$). Upon *GPRC5C* overexpression, the migration rate recovered to 47.31% ± 5.31% (adj. $p = 0.0097$). Similarly, *GPRC5C* rescued the invasive defect in *ARID4B*-knockdown cells (Figure 7e). The number of invading cells decreased from 69.93 ± 6.40 (LvshNC + Vector) to 26.27 ± 2.75 (LvshARID4B + Vector; −62.4%, adj. $p < 0.0001$). Overexpression of *GPRC5C* restored invasion to 63.87 ± 3.58, representing a 96.3% recovery relative to the LvshARID4B + Vector group (adj. $p = 0.0001$). Consistent with these functional changes, *GPRC5C* overexpression led to upregulation of the mesenchymal marker SNAIL and downregulation of the epithelial marker E-cadherin, indicating reversal of the EMT suppression induced by *ARID4B* knockdown (Figure 7d). Collectively, these findings demonstrate that the oncogenic effects of *ARID4B* in promoting stemness, migration, invasion, and EMT in LUAD cells are primarily mediated through its transcriptional target, *GPRC5C*.

DISCUSSION

LUAD remains a major therapeutic challenge because of its propensity for metastasis and recurrence. In this study, we identify *ARID4B* as a key epigenetic driver of LUAD progression and uncover a previously unrecognized regulatory axis between *ARID4B* and the orphan receptor *GPRC5C*. Our findings provide multilevel evidence,

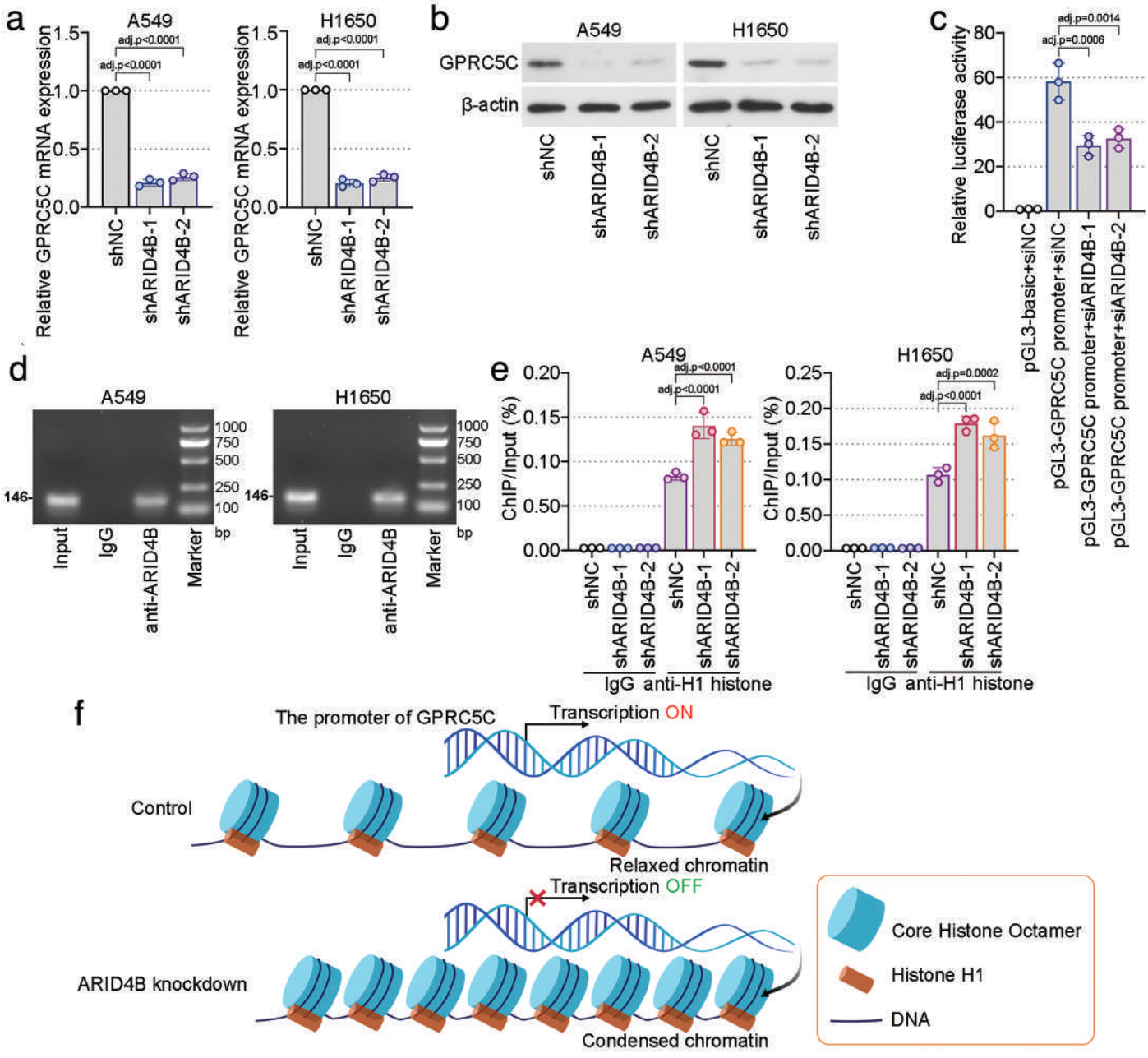

FIG. 6. *ARID4B* promotes the transcriptional activation of *GPRC5C*. (a, b) Real-time polymerase chain reaction and Western blot analysis of *GPRC5C* expression in tumor cells with *ARID4*B knockdown. (c) The dual-luciferase assay was performed 48 h after transfection with the indicated *GPRC5C* promoter fragments and *ARID4B* knockdown vector or empty vector. (d) Binding of *ARID4B* to the *GPRC5C* promoter was verified by ChIP experiments. (e) The effect of *ARID4B* on the binding of H1 histone to the *GPRC5C* promoter was detected by ChIP experiments. (f) Mechanism diagram of the influence of *ARID4B* on the transcription of *GPRC5C*. Data are expressed as mean ± standard deviation (n = 3, biological replicates). Comparisons among multiple groups were performed by one-way ANOVA followed by Tukey's post-hoc test; the *p* values shown in the figure are adjusted *p* values (adj. *p*) after Bonferroni correction.

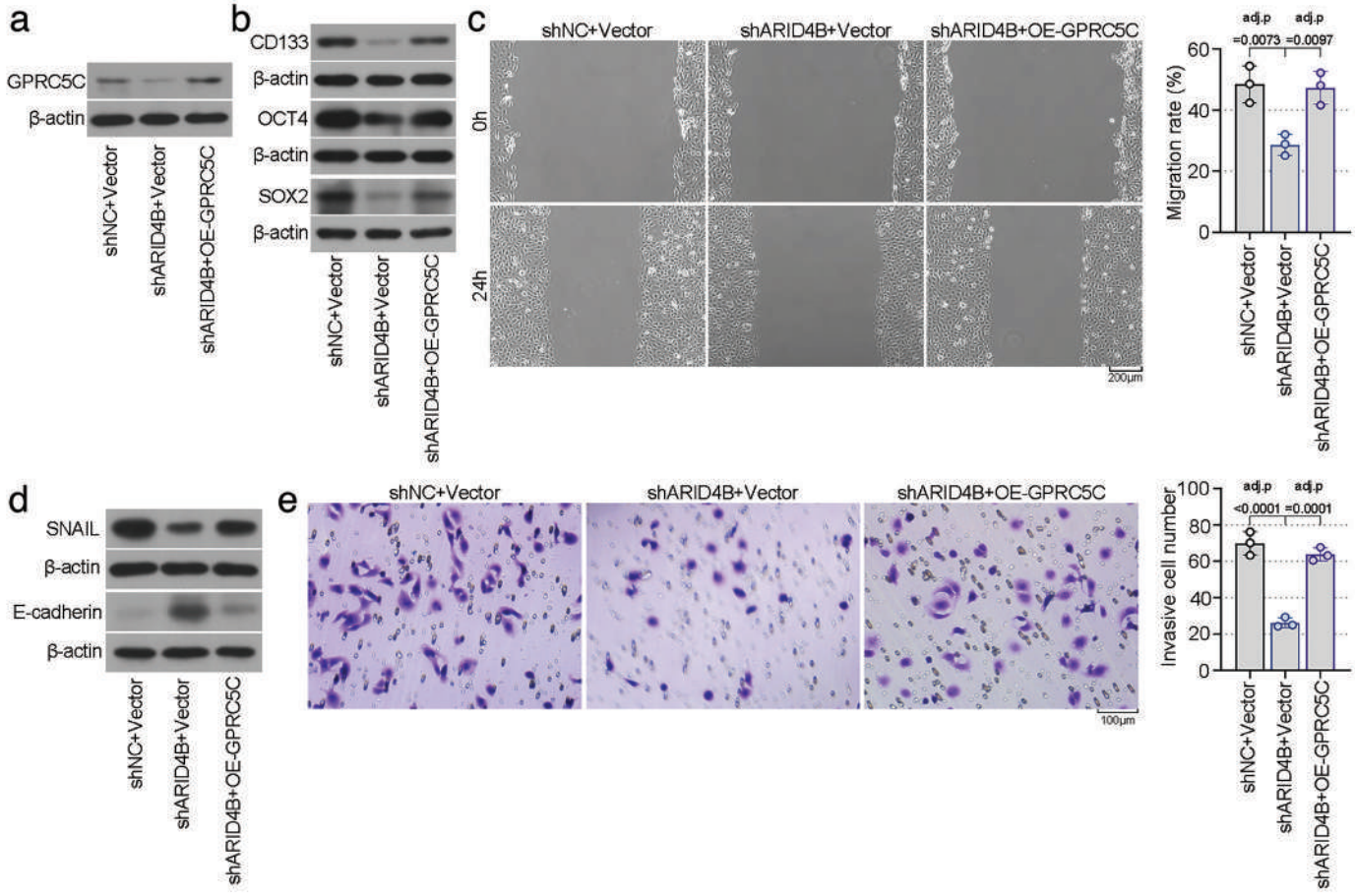

FIG. 7. *ARID4B* regulates the expression of *GPRC5C* to influence the malignant phenotype of lung adenocarcinoma (LUAD) cells. (a) The *GPRC5C* overexpression plasmid was transfected into H1650 cells with stable knockdown of *ARID4B*. Western blot was further used to detect the expression of *GPRC5C* after 48 h. (b) Western blot analysis of *CD133*, *OCT4* and *SOX2* expression in tumor cells. (c) Photographs showed cell migration before and after injury under the microscope at 100 × magnification field. Quantification of cell migration by measuring wound closure areas before and after injury. (d) Western blot analysis of E-cadherin and SNAIL expression in cells. (e) The invasive ability of LUAD cells was evaluated through the transwell assay (crystal violet staining × 200). Data are expressed as mean ± standard deviation (n = 3, biological replicates, all experimental groups within a given biological replicate were processed and assayed in parallel under identical conditions). Comparisons among multiple groups were performed by one-way ANOVA followed by Tukey's post-hoc test; the *p* values shown in the figure are adjusted *p* values (adj. *p*) after Bonferroni correction.

ranging from bioinformatic analyses to *in vivo* models, supporting the functional significance of *ARID4B* in promoting stemness, EMT, and metastasis.

Chromatin remodeling proteins are a class of complexes that control gene expression by altering chromatin structure, specifically, the packing density of DNA and histones.[17] Rather than modifying the DNA sequence itself, these proteins regulate gene activation and repression through epigenetic mechanisms.[18,19] Dysfunction of chromatin remodelers often results in abnormal oncogene activation or tumor suppressor gene silencing, thereby driving tumor initiation, progression, and metastasis.[20,21] *ARID4B*, a classical chromatin remodeling factor, contains both a Tudor domain and a chromodomain, which may are thought to facilitate the assembly of chromatin remodeling complexes.[22] Numerous previous studies have confirmed the oncogenic role of *ARID4B* in multiple tumor types. Consistent with these reports, we confirmed *ARID4B* is highly expressed in LUAD tissues and that its elevated expression is associated with poor prognosis.

We next examined the role of *ARID4B* in regulating EMT and CSC properties in LUAD cells. Wang et al.[23] reported that *ARID4B* promotes invasion and EMT of melanoma by activating the PI3K/AKT signaling pathway. Similarly, downregulation of *ARID4B* has been shown to inhibit tumor cell migration and proliferation in hepatocellular carcinoma.[24] Our findings are consistent with these reports and further underscore the critical role of *ARID4B* in EMT regulation. Notably, the reciprocal regulation of E-cadherin and SNAIL following *ARID4B* knockdown strongly supports its involvement in key metastatic processes. Importantly, our study extends these findings by delineating its role in lung cancer stemness. We demonstrate that *ARID4B* knockdown suppresses key stemness markers, including

CD133, *OCT4*, and *SOX2*, and significantly reduces tumorsphere formation. These results implicate *ARID4B* in the maintenance of CSC populations, which are closely associated with therapeutic resistance and disease relapse, thereby expanding the growing evidence linking chromatin remodelers to CSC regulation.

A further novel aspect of this study is the mechanistic dissection of the *ARID4B* and *GPRC5C* relationship. *GPRC5C* is a functionally important orphan receptor that is widely expressed in organs such as the lung and kidney.[25] Although *GPRC5C* remains relatively understudied, it has attracted increasing attention in tumor biology. Recent studies have implicated *GPRC5C* in metabolic reprogramming in leukemia and in promoting invasion in pancreatic cancer.[15,16] Based on ChIP-seq data from prostate cancer demonstrating *ARID4B* binding to the *GPRC5C* promoter,[13] we further confirmed that *ARID4B* directly binds to the *GPRC5C* promoter and transcriptionally activates it expression by displacing histone H1, a well-known chromatin-compacting factor. This finding is consistent with the established role of *ARID4B* in disrupting histone H1-mediated chromatin condensation.[26] Such epigenetic relaxation of chromatin structure facilitates gene activation and reveals a precise mechanistic explanation for how *ARID4B* exerts its oncogenic effects. Furthermore, our rescue experiments functionally validated *GPRC5C* as a critical downstream mediator of *ARID4B*-driven malignancy. Re-expression of *GPRC5C* reversed the suppression of stemness, migration, invasion, and EMT induced by *ARID4B* knockdown, underscoring the central role of this regulatory axis.

Despite these insights, several questions warrant further investigation. Although the clinical relevance of *ARID4B* was preliminarily assessed using public datasets, validation in large independent LUAD patient cohort is needed to firmly establish its prognostic and biomarker potential. In addition, the upstream regulatory mechanisms responsible for *ARID4B* overexpression in LUAD remain unclear. Ding et al.[27] reported that STAT3 indirectly regulates *ARID4B*-related signaling through activation of the lncRNA ZBED3-AS1, thereby promoting melanoma progression.[23] Notably, STAT3 has also been shown to exacerbate LUAD metastasis.[27] This findings raise the possibility that the high expression of *ARID4B* in LUAD is related to the regulation of transcription factors. Several mechanistic questions regarding *GPRC5C* also remain unresolved. As an orphan receptor, the endogenous ligand of *GPRC5C* has yet to be identified. Recent evidence indicates that *GPRC5C* drives branched-chain amino acid metabolic reprogramming in leukemia, promoting leukemia stem cell survival.[15] Given that metabolic reprogramming is an important feature of LUAD,[28] we speculate that branched-chain amino acids or their metabolic intermediates may serve as potential ligands for *GPRC5C*. If *GPRC5C* can sense changes in branched-chain amino acid levels and activate downstream signaling pathways such as PI3K/AKT or MAPK, which are frequently dysregulated in LUAD and closely linked to EMT and stemness,[24,29-31] this may form a "metabolite-receptor-signaling pathway" regulatory axis that drives LUAD malignancy. Finally, although our functional and mechanistic investigations were conducted in two widely used LUAD cell lines, A549 and H1650, the molecular heterogeneity of LUAD neccessitates broader validation. Future studies will aim to validate our findings in additional LUAD cell lines and patient-derived primary tumor cells to further confirm the broader relevance of this regulatory axis. These issues will be the focus of our future research.

In summary, our study identifies *ARID4B* as a key epigenetic regulator that enhances LUAD aggressiveness through transcriptional activation of *GPRC5C*. These insights deepen our understanding of LUAD biology and highlight a potential therapeutic axis for a cancer type in urgent need of more effective treatment strategies. Targeting this axis may benefit patients with high *ARID4B* expression, particularly those with advanced or metastatic disease.

Ethics Committee Approval: This study was approved by the Clinical Research Ethics Committee of the People's Hospital of Xinjiang Uygur Autonomous Region (approval number: KY2024052105; date: 21.05.2024).

Informed Consent: Not applicable.

Data Sharing Statement: The data that support the findings of this study are available from the corresponding author upon reasonable request.

Authorship Contributions: Concept- G.H.; Design- G.H., S.F.; Supervision- L.G.; Funding- L.G.; Materials- S.F., L.X.; Data Collection or Processing- L.X.; Analysis and/or Interpretation- X.Z.; Literature Review- X.Z.; Writing- G.H.; Critical Review- L.G.

Conflict of Interest: The authors declare that they have no conflict of interest.

Funding: This research was funded by the Natural Science Foundation of Xinjiang Uygur Autonomous Region (Grant No. 2024D01A114).

REFERENCES

1. Sung H, Ferlay J, Siegel RL, et al. Global Cancer Statistics 2020: GLOBOCAN Estimates of Incidence and Mortality Worldwide for 36 Cancers in 185 Countries. *CA Cancer J Clin.* 2021;71:209-249. [CrossRef]
2. Siegel RL, Giaquinto AN, Jemal A. Cancer statistics, 2024. *CA Cancer J Clin.* 2024;74:12-49. Erratum in: *CA Cancer J Clin.* 2024;74:203. [CrossRef]
3. Imielinski M, Berger AH, Hammerman PS, et al. Mapping the hallmarks of lung adenocarcinoma with massively parallel sequencing. *Cell.* 2012;150:1107-1120. [CrossRef]
4. Zhang Y, Wang LF, Gao JH, et al. Clinical significance of epithelial-mesenchymal transition-related molecules in lung adenocarcinoma. *Curr Oncol.* 2019;26:e121-e127. [CrossRef]
5. Li Y, Zhang X, Zhu S, et al. HDAC10 regulates cancer stem-like cell properties in KRAS-driven lung adenocarcinoma. *Cancer Res.* 2020;80:3265-3278. [CrossRef]
6. Du B, Shim JS. Targeting Epithelial-Mesenchymal Transition (EMT) to overcome drug resistance in cancer. *Molecules.* 2016;21:965. [CrossRef]
7. Lytle NK, Barber AG, Reya T. Stem cell fate in cancer growth, progression and therapy resistance. *Nat Rev Cancer.* 2018;18:669-680. [CrossRef]
8. Kim BN, Ahn DH, Kang N, et al. TGF-β induced EMT and stemness characteristics are associated with epigenetic regulation in lung cancer. *Sci Rep.* 2020;10:10597. [CrossRef]
9. Okawa R, Banno K, Iida M, et al. Aberrant chromatin remodeling in gynecological cancer. *Oncol Lett.* 2017;14:5107-5113. [CrossRef]
10. Sinha S, Molla S, Kundu CN. PARP1-modulated chromatin remodeling is a new target for cancer treatment. *Med Oncol.* 2021;38:118. [CrossRef]
11. Goldberger N, Walker RC, Kim CH, Winter S, Hunter KW. Inherited variation in miR-290 expression suppresses breast cancer progression by targeting the metastasis susceptibility gene Arid4b. *Cancer Res.* 2013;73:2671-2681. [CrossRef]
12. Cao J, Gao T, Stanbridge EJ, Irie R. RBP1L1, a retinoblastoma-binding protein-related gene encoding an antigenic epitope abundantly expressed in human carcinomas and normal testis. *J Natl Cancer Inst.* 2001;93:1159-1165. [CrossRef]
13. Wu RC, Young IC, Chen YF, et al. Identification of the PTEN-ARID4B-PI3K pathway reveals the dependency on ARID4B by PTEN-deficient prostate cancer. *Nat Commun.* 2019;10:4332. [CrossRef]

14. Winter SF, Lukes L, Walker RC, Welch DR, Hunter KW. Allelic variation and differential expression of the mSIN3A histone deacetylase complex gene Arid4b promote mammary tumor growth and metastasis. *PLoS Genet.* 2012;8:e1002735. [CrossRef]
15. Zhang YW, Velasco-Hernandez T, Mess J, et al. GPRC5C drives branched-chain amino acid metabolism in leukemogenesis. *Blood Adv.* 2023;7:7525-7538. [CrossRef]
16. Liu WJ, Lu J, Zhou WX, Liu JZ, Zhou L. MLH1 inhibits metastatic potential of pancreatic ductal adenocarcinoma via downregulation of GPRC5C. *Lab Invest.* 2024;104:102107. [CrossRef]
17. Mashtalir N, D'Avino AR, Michel BC, et al. Modular organization and assembly of SWI/SNF family chromatin remodeling complexes. *Cell.* 2018;175:1272-1288.e20. [CrossRef]
18. Song Q, Hou Y, Zhang Y, et al. Integrated multi-omics approach revealed cellular senescence landscape. *Nucleic Acids Res.* 2022;50:10947-10963. [CrossRef]
19. Sahu RK, Dhakshnamoorthy J, Jain S, et al. Nucleosome remodeler exclusion by histone deacetylation enforces heterochromatic silencing and epigenetic inheritance. *Mol Cell.* 2024;84:3175-3191.e8. [CrossRef]
20. Bakr A, Della Corte G, Veselinov O, et al. ARID1A regulates DNA repair through chromatin organization and its deficiency triggers DNA damage-mediated anti-tumor immune response. *Nucleic Acids Res.* 2024;52:5698-5719. [CrossRef]
21. Tsuda M, Fukuda A, Kawai M, Araki O, Seno H. The role of the SWI/SNF chromatin remodeling complex in pancreatic ductal adenocarcinoma. *Cancer Sci.* 2021;112:490-497. [CrossRef]
22. Lin C, Song W, Bi X, et al. Recent advances in the ARID family: focusing on roles in human cancer. *Onco Targets Ther.* 2014;7:315-324. [CrossRef]
23. Wang Y, Lou N, Zuo M, et al. STAT3-induced ZBED3-AS1 promotes the malignant phenotypes of melanoma cells by activating PI3K/AKT signaling pathway. *RNA Biol.* 2021;18:355-368. [CrossRef]
24. Akaoka M, Yanagaki M, Kubota H, et al. ARID4B promotes the progression of hepatocellular carcinoma through the PI3K/AKT pathway. *Ann Surg Oncol.* 2025;32:3009-3018. [CrossRef]
25. Kawabata Y, Takai S, Sanematsu K, et al. The G protein-coupled receptor GPRC5C is a saccharide sensor with a novel 'off' response. *FEBS Lett.* 2023;597:2006-2016. [CrossRef]
26. Hergeth SP, Schneider R. The H1 linker histones: multifunctional proteins beyond the nucleosomal core particle. *EMBO Rep.* 2015;16:1439-1453. [CrossRef]
27. Ding J, Wang X, Yang H, et al. IGF2BP3 triggers STAT3 pathway by stabilizing SRC RNA in an m6A-dependent manner to promote lymphatic metastasis in LUAD. *Cancer Sci.* 2025;116:936-950. [CrossRef]
28. Nie M, Yao K, Zhu X, et al. Evolutionary metabolic landscape from preneoplasia to invasive lung adenocarcinoma. *Nat Commun.* 2021;12:6479. [CrossRef]
29. Wei C, Dong X, Lu H, et al. LPCAT1 promotes brain metastasis of lung adenocarcinoma by up-regulating PI3K/AKT/MYC pathway. *J Exp Clin Cancer Res.* 2019;38:95. [CrossRef]
30. Zheng Y, You H, Duan J, et al. Centromere protein N promotes lung adenocarcinoma progression by activating PI3K/AKT signaling pathway. *Genes Genomics.* 2022;44:1039-1049. [CrossRef]
31. Wang S, Tong X, Li C, et al. Quaking 5 suppresses TGF-β-induced EMT and cell invasion in lung adenocarcinoma. *EMBO Rep.* 2021;22:e52079. [CrossRef]